

23  
RECORDS ADMINISTRATION  
  
ACUC

ACC # 734721  
DP-MS-82-96, Rev. 5/83

**PHYSICAL MODELING OF A GLASS MELTER DESIGNED FOR  
VITRIFICATION OF DEFENSE WASTE**

by

Kenneth R. Routt

E. I. du Pont de Nemours & Co.  
Savannah River Laboratory  
Aiken, South Carolina 29808

SRL  
RECORD COPY

A paper proposed for presentation at the **Second International Symposium on Ceramics in Nuclear Waste Management**, Chicago, Illinois, April 23-27, 1983 and for publication in the **Proceedings of the American Ceramic Society Annual Meeting**

---

This paper was prepared in connection with work done under Contract No. DE-AC09-76SR00001 with the U.S. Department of Energy. By acceptance of this paper, the publisher and/or recipient acknowledges the U.S. Government's right to retain a nonexclusive, royalty-free license in and to any copyright covering this paper, along with the right to reproduce and to authorize others to reproduce all or part of the copyrighted paper.

This document was prepared in conjunction with work accomplished under Contract No. DE-AC09-76SR00001 with the U.S. Department of Energy.

### **DISCLAIMER**

This report was prepared as an account of work sponsored by an agency of the United States Government. Neither the United States Government nor any agency thereof, nor any of their employees, makes any warranty, express or implied, or assumes any legal liability or responsibility for the accuracy, completeness, or usefulness of any information, apparatus, product or process disclosed, or represents that its use would not infringe privately owned rights. Reference herein to any specific commercial product, process or service by trade name, trademark, manufacturer, or otherwise does not necessarily constitute or imply its endorsement, recommendation, or favoring by the United States Government or any agency thereof. The views and opinions of authors expressed herein do not necessarily state or reflect those of the United States Government or any agency thereof.

This report has been reproduced directly from the best available copy.

Available for sale to the public, in paper, from: U.S. Department of Commerce, National Technical Information Service, 5285 Port Royal Road, Springfield, VA 22161, phone: (800) 553-6847, fax: (703) 605-6900, email: [orders@ntis.fedworld.gov](mailto:orders@ntis.fedworld.gov) online ordering: <http://www.ntis.gov/ordering.htm>

Available electronically at <http://www.doe.gov/bridge>

Available for a processing fee to U.S. Department of Energy and its contractors, in paper, from: U.S. Department of Energy, Office of Scientific and Technical Information, P.O. Box 62, Oak Ridge, TN 37831-0062, phone: (865) 576-8401, fax: (865) 576-5728, email: [reports@adonis.osti.gov](mailto:reports@adonis.osti.gov)

**PHYSICAL MODELING OF A GLASS MELTER DESIGNED FOR  
VITRIFICATION OF DEFENSE WASTE\***

by Kenneth R. Routt

E. I. du Pont de Nemours & Co.  
Savannah River Laboratory  
Aiken, South Carolina 29808

**ABSTRACT**

Various conservation equations were written in dimensionless form and used as a design basis for a physical model of a proposed glass melter for immobilization of liquid radioactive waste at the Savannah River Plant. Model predictions are compared with actual melter data.

**I. Introduction**

A key step in the process of converting liquid radioactive waste stored at the Savannah River Plant into an immobile glass product is the design and successful operation of a glass melter in which the waste and glass forming materials (frit) are mixed at a high temperature to form a homogeneous glass product.

However, the high operating temperature of such a melter (1150°C) makes it difficult to determine important characteristics of the glass/melter system, such as glass flow patterns and melter voltage profiles. Physical models of glass melters can be used to obtain this data, if they are sufficiently similar to an actual melter. The theoretical relationships necessary to design, operate, and interpret data from a physical model of a glass melter are presented in this paper and applied, as an example, to an actual glass melter operated at the Savannah River Plant.

---

\* The information contained in this article was developed during the course of work under Contract No. DE-AC09-76SR00001 with the U.S. Department of Energy.

## II. Scaling Relationships

The glass melter to be modeled consisted of a ceramic lined, water-cooled, steel vessel of cylindrical geometry with four rod electrodes (Figure 1). The governing equations for such a melter consist of conservation of mass, momentum, energy, and electrical charge in three-dimensional, cylindrical coordinates. A detailed examination of these equations in dimensionless form has been previously presented<sup>1</sup> and will not be repeated here. Instead, a simple listing of important dimensionless quantities (denoted by asterisks) useful for modeling purposes is given below.

From the definition of dimensionless coordinates one has

$$r^* = \frac{r}{R}, \quad \theta^* = \theta, \quad z^* = \frac{z}{R} \quad (1)$$

From the dimensionless mass and momentum equations one has

$$v_r^* = \frac{Rv_r}{\alpha_o}, \quad v_\theta^* = \frac{Rv_\theta}{\alpha_o}, \quad v_z^* = \frac{Rv_z}{\alpha_o} \quad (2)$$

$$P^* = \frac{R^2 g_o P}{\alpha_o \mu_o}, \quad N_{Pr} = \frac{v_o}{\alpha_o}, \quad N_{Ga} = \frac{R^3 g}{v_o^2} \quad (3)$$

$$N_{Ra} = \frac{R^2 g \beta (T_1 - T_o)}{v_o \alpha_o}, \quad W^* = \frac{R^2 W}{\alpha_o \rho_o}, \quad \left( \frac{\mu}{\mu_o} \right) \quad (4)$$

From the dimensionless energy equation one has

$$\left( \frac{k}{k_o} \right), \quad T^* = \frac{T - T_o}{T_1 - T_o}, \quad Q^* = \frac{R^2 Q}{k_o (T_1 - T_o)} \quad (5)$$

$$Q_t^* = \frac{Q_t}{k_o (T_1 - T_o) R} \quad (6)$$

From the dimensionless charge equation one has

$$\left(\frac{\sigma}{\sigma_0}\right), \quad v^* = \frac{v}{v_0}, \quad Q_e^* = \frac{R^2 Q_e}{\sigma_0 v_0} \quad (7)$$

$$I^* = \frac{I}{\sigma_0 v_0 R}, \quad J^* = \frac{RJ}{\sigma_0 v_0}, \quad P^* = \frac{R^2 P}{\sigma_0 v_0^2} \quad (8)$$

$$P_t^* = \frac{P_t}{R \sigma_0 v_0^2}, \quad R_e^* = R \sigma_0 R_e, \quad v_0 = \left[ \frac{k_0 (T_1 - T_0)}{\sigma_0} \right]^{1/2}. \quad (9)$$

Modeling theory requires that the dimensionless ratios given in Equations (1) through (9) be the same in both the model and the glass melter. If this condition is met, then the model will be governed by the same dimensionless equations as the melter and it becomes possible to use the model as a useful tool for predicting the behavior of the glass melter, and thus evaluate its design.

To obtain a unique solution to the governing partial differential equations, suitable boundary conditions must be specified. Furthermore they must be the same in both the model and the melter. These boundary conditions are discussed in detail elsewhere<sup>1</sup> and fortunately, many of them are usually automatically satisfied by the construction features of the model. Those that are not are discussed below.

When operating the melter under feeding conditions, a mass balance at the melt surface leads to the definition of the dimensionless feed rate

$$f^* = \frac{f}{\rho_0 R \alpha_0} \quad (10)$$

which must be satisfied by the model.

The dimensionless energy equation requires that the temperature gradients at the sides, bottom, and top of the melt pool be specified as

$$\frac{\partial T^* (1, \theta^*, z^*)}{\partial r^*} = \frac{-U_s R}{k} [T^* (1, \theta^*, z^*) - T_c^*] \quad (11)$$

$$\frac{\partial T^* (r^*, \theta^*, Z/R)}{\partial z^*} = \frac{-U_b R}{k} [T^* (r^*, \theta^*, Z/R) - T_c^*] \quad (12)$$

$$\frac{\partial T^* (r^*, \theta^*, 0)}{\partial z^*} = \frac{-R}{(T_1 - T_0)k} \left( \frac{q}{A} \right)_f = - \left( \frac{q}{A} \right)_f^* \quad (13)$$

### III. Similarity Requirements for Modeling

The dependent variables in the conservation equations are the three-dimensional distributions of pressure  $p^*$ , velocity  $v_r^*$ ,  $v_\theta^*$ ,  $v_z^*$ , temperature  $T^*$ , and voltage  $V^*$ . It is these quantities about which information is sought in the model so that they can be scaled to the actual glass melter.

Thus the model ideally must satisfy all of the following requirements when compared to the melter:

1. All dimensionless coordinates must match, i.e.,  $r^*$ ,  $\theta^*$ ,  $z^*$  with respect to model depth, radius, electrode geometry and placement, etc. This is called geometric similarity.
2. The dimensionless numbers  $W^*$ ,  $N_{Pr}$ ,  $N_{Ga}N_{Pr}$ ,  $N_{Ra}$ ,  $Q^*$ , and  $Q_e^*$  must match.
3. The physical property ratios  $\left( \frac{\mu}{\mu_o} \right)$ ,  $\left( \frac{k}{k_o} \right)$ , and  $\left( \frac{\sigma}{\sigma_o} \right)$  must match.

4. The boundary conditions must match over the operating temperature range of the model.

If these requirements are met, the dimensionless values of  $I^*$ ,  $J^*$ ,  $P^*$ ,  $P_t^*$ ,  $Q_t^*$ , and  $Re^*$  will also match.

#### IV. Melter Construction

The glass melter (Figure 1) was a cylindrical vessel with joule heat provided by four, top entering, rod electrodes. Simulated waste glass was continuously fed into the melter from the top and brought to a nominal operating temperature of 1150°C before being discharged into steel canisters.

A mixture of borosilicate frit plus simulated radioactive waste was initially designed for testing in the melter. The desired operating temperature range for the melter was 1050 to 1150°C. The reference temperature for the physical properties of the glass was chosen to be  $T_0 = 1100^\circ\text{C}$ .

#### V. Model Construction and Operation

Other articles have appeared in the literature regarding physical modeling of electrically heated glass melters using glycerine +  $\text{LiCl}$ .<sup>2-5</sup>

The scale  $s$  of the model can be defined as any convenient dimension of the model, e.g., melt pool radius  $R$ , divided by the same corresponding dimension in the actual melter. The scale of the model was chosen to be  $s = 1/2$  in order to achieve a good match of the physical property ratios over an anticipated model operating range of

approximately 25 to 35°C. The reference temperature for the fluid properties of the model was chosen to be  $T_0 = 30^\circ\text{C}$ . Glycerine + 10 wt % LiCl was chosen for the model fluid.

The model was constructed as an acrylic, cylindrical tank placed inside a larger, rectangular tank (Figures 2 and 3). Note that only the melt pool was represented since the slanted riser was omitted.

The model depth and radius, as well as electrode geometry and placement were all scaled to achieve geometric similarity. The electrodes were made from copper and connected to a two-phase electrical power supply similar to that of the melter.

Control of the boundary conditions for the energy equation on the sidewalls and bottom was achieved by use of a single water jacket since  $U_s \cong U_b$  in the design of the glass melter. A separate water jacket at the top of the model was used to control the thermal boundary condition at the top.

A good match of the Prandtl number  $N_{Pr}$  was not possible in the model. However, since the Prandtl numbers for both the glass and the model fluid were large and appeared in the denominators of the dimensionless equations,<sup>1</sup> this error was not thought to be serious.

The term  $N_{Ga}N_{Pr}$  is the dimensionless result of the gravitational force acting on the glass pool.<sup>1</sup> If the glass pool circulates only due to natural convection, i.e., no bubblers or mechanical stirrers are used, then this term is virtually cancelled from the equation by simply approximating the pressure  $p^*$  as the gravitational force. Thus it was not necessary to match  $N_{Ga}N_{Pr}$  in the model.

The Rayleigh number  $N_{Ra}$  is the dimensionless result of buoyant forces acting in the glass pool.<sup>1</sup> Since this is the dominant mechanism for glass circulation, the model must match  $N_{Ra}$ .

Temperature and voltage profiles were measured in the model by use of iron-constantan thermocouples inserted into the model fluid through acrylic sleeves in the top cooling jacket. Heat shrinkable tubing was used to electrically isolate the thermocouples from the model fluid and prevent distortion of the voltage distribution. However, the lower tip of the thermocouples was left exposed so that the thermocouples could also be used as point sensors to measure voltage.

Powdered anthracene ( $C_{14}H_{10}$ ) was sieved to obtain particles <149 microns (100 mesh) for use as neutrally buoyant, tracer particles for mapping the velocity distribution  $v^*$  in the model. Particles in a vertical plane were illuminated by use of a collimated light source passing up through the bottom of the model in an otherwise dark room. Movement of the tracer particles was recorded using a Polaroid® (The Polaroid Corp.) MP-4 camera and Polaroid® Type 55, ASA 50 film. Film exposure time was generally 10 to 30 seconds, while tracer particle velocities were on the order of several cm/hr.

## VI. Results

The cylindrical coordinate system used for the glass melter is shown in Figure 4. A radial voltage profile taken through the vertical plane of electrodes B and D is shown in Figure 5 and was the same when measured in the vertical plane of electrodes A and C due to symmetry.

The electrical power density is proportional to the square of the voltage gradient in the  $r$ ,  $\theta$ , and  $z$  directions.<sup>1</sup> Figure 5 shows that the voltage gradient in the upper 70 to 80 cm of the melt pool is nearly uniform. Near the bottom of the melt pool, the square of the radial voltage gradient is only about 20% of that in the upper portion of the melt pool. Figure 6 shows the same type of data taken in a plane rotated  $45^\circ$  away from the B-D electrode pair. The maximum voltage at all depths in the glass pool dropped significantly as well as the radial voltage gradient. The square of the radial voltage gradient in the upper 70 to 80 cm of the melt pool is only 15 to 30% of that in the plane of Figure 5. Again the radial component of the power density is low near the bottom of the melt pool, but is not much different than that in Figure 5 at the same glass depth.

Figure 7 shows azimuthal voltage profiles measured by sweeping around a circle which passed through each of the four electrodes. The square of the azimuthal voltage gradient is about 20 to 25% of the square of the radial voltage gradient in the upper part of the B-D electrode plane. Other azimuthal voltage data were similar to Figure 7 but showed an increasingly lower voltage gradient at decreasing values of  $r$ .

Typical vertical voltage profiles are shown in Figure 8, and are essentially flat with little gradient in the  $z$ -direction except below the bottom of the electrodes. Here the square of the vertical voltage gradient near the center of the melt pool (small  $r$ ) is about 10 to 15%

of the square of the radial voltage gradient in the upper part of the B-D electrode plane, but ranges from 30 to 90% at values of  $r$  close to the electrode.

The voltage profiles may be summarized by noting that the largest contribution to the local power density occurs due to a strong radial voltage gradient along a straight line path between each of the two diametrically opposite electrode pairs (A-C and B-D). Contributions due to azimuthal and vertical voltage gradients are substantially less. The local power density near the bottom of the melt pool appears quite low as indicated by relatively small voltage gradients in this region in Figures 5-8.

Figure 9 shows that the radial temperature profiles are relatively flat in the B-D electrode plane. The lower 20 cm of the melt pool appears to be dominated by conduction since no evidence of a thermal boundary layer exists near the sidewalls and the profile is peaked near the center ( $r = 0$ ). In the upper half of the tank, natural convection appears to be substantial since the strong temperature gradient at the sidewalls suggests the presence of a thermal boundary layer and the temperature profiles are flat near the center ( $r = 0$ ). Radial temperature profiles taken in other vertical planes appeared similar to Figure 9.

Typical azimuthal temperature profiles are shown in Figure 10 and appear very flat at all values of  $z$ . A typical vertical temperature profile is shown in Figure 11 and indicates that the temperature drops approximately linearly with increasing depth but takes an even more

rapid drop below the bottom of the electrodes. Recalling that the intended operating range was 1050 to 1150°C, note that the model predicts a bottom temperature of about 937°C and a peak temperature of 1140°C. After the modeling program was terminated, the reference glass composition for the melter was changed to a less viscous composition (from 4.3 Pa-s to 1.7 Pa-s at 1150°C). When the melter was subsequently started up, the actual vertical temperature profile was measured (Figure 11). Note that the actual operating temperature range (920 to 1135°C) was predicted quite closely by the model although the shape of the temperature profile from the model was somewhat different. However, this difference is consistent qualitatively with what one would expect by the lower viscosity of the new glass composition.

The velocity distribution in the vertical plane of one of the electrodes is shown in Figure 12, and is typical near each of the four electrodes. Very slow moving glass occurs near the melter floor, which is consistent with the estimates of the electrical power density from the voltage profiles as well as the relatively low temperatures predicted by the temperature profiles. The fastest moving glass occurs behind each electrode apparently due to strong heating near the electrode accompanied by cooling along the melter sidewall.

A summary of electrical parameters predicted for the melter is given in Table I. Data from the model were scaled up for a melt rate of 40-51 kg/hr. Actual data taken from the melter are for a slightly different glass composition (and presumably electrical conductivity) at a melt rate of 189 kg/hr. Thus it is difficult to assess the accuracy

of the model with respect to volts, amps, and resistance, although the model predictions are definitely reasonable. The model does predict a somewhat higher power level than was measured in the melter.

## VII. Conclusions

Physical modeling principles applied to the simulation of a glass melter designed for processing of radioactive waste glass appear to be excellent tools for evaluating melter design and performance. Models can certainly provide information in greater detail regarding temperature and voltage profiles than is usually obtainable in an actual glass melter. Furthermore, the measurement of velocity profiles in an actual melter is not possible but can be easily performed in a model.

A model can not only be used to increase general understanding of the melting process, but it can also provide specific suggestions for improvement in melter design. As a result of the modeling results presented here, for example, it was recommended that the bottom heat transfer coefficient  $U_b$  be decreased in future melter designs in order to raise the temperature of the glass near the bottom of the melt pool. It was also recommended that alternate electrode configurations be examined in order to provide flexibility in control of the electrical power density in the vertical direction. Future work with physical models will study these recommendations in detail.

### VIII. Nomenclature

$f$	= mass feed rate of material at the melt surface (kg/s)
$g$	= local gravitational constant ( $m^2/s$ )
$g_0$	= standard gravitational constant ( $kg-m/s^2-N$ )
$I$	= electrode current (A)
$J$	= current flux ( $A/cm^2$ )
$k$	= thermal conductivity of the glass at any temperature $T$ ( $W/m-K$ )
$k_0$	= thermal conductivity of the glass at temperature $T_0$ ( $W/m-K$ )
$N_{Ga}$	= Galileo number
$N_{Pr}$	= Prandtl number
$N_{Ra}$	= Rayleigh number
$p$	= pressure in the glass pool at any $r, \theta, z$ (Pa)
$P$	= electrical power density ( $kW/m^3$ )
$P_t$	= total electrical power (kW)
$(q/A)_f$	= heat flux to the feedpile ( $W/m^2$ )
$Q$	= thermal energy source term ( $kW/m^3$ )
$Q_e$	= volumetric electrical charge injection rate ( $C/m^3-s$ )
$Q_t$	= total thermal power (kW)
$r$	= radial coordinate direction (m)
$R$	= radius of the melt pool (m)
$R_e$	= equivalent resistance between an electrode pair ( $\Omega$ )
$s$	= scale factor of model
$T$	= glass temperature at any $r, \theta, z$ (K)
$T_0$	= reference temperature for definition of physical properties, e.g., midpoint of intended operating temperature range (K)
$T_1$	= glass temperature at a selected reference point, e.g., the hottest point in the melt pool (K)

$T_c$	= average temperature of coolant used on melter vessel (K) or ambient temperature if vessel is uncooled (K)
$T^+$	= $(T - T_{\min}) / (T_{\max} - T_{\min})$ , used for plotting purposes
$U_b$	= heat transfer coefficient for bottom of melt pool ( $W/m^2-K$ )
$U_s$	= heat transfer coefficient for submerged sidewall of melt pool ( $W/m^2-K$ )
$v_r, v_\theta, v_z$	= glass velocity components in the r, $\theta$ , and z directions, respectively (m/s)
$V$	= electrical potential in the glass pool at any r, $\theta$ , z (V)
$V_0$	= reference electrical potential (V)
$W$	= volumetric mass injection rate, usually zero ( $kg/m^3-s$ )
$z$	= vertical coordinate direction (m)
$z^+$	= $z^* R/Z$ , used for plotting purposes
$Z$	= depth of glass pool (m)
$\alpha_0$	= glass thermal diffusivity at temperature $T_0$ ( $m^2/s$ )
$\theta$	= azimuthal coordinate direction (rad)
$\theta^+$	= $\theta/2\pi$ , used for plotting purposes
$\mu$	= glass viscosity at any temperature T (Pa-s)
$\mu_0$	= glass viscosity at temperature $T_0$ (Pa-s)
$\rho_0$	= glass density at temperature $T_0$ ( $kg/m^3$ )
$\sigma$	= electrical conductivity of glass at any temperature T (S/m)
$\sigma_0$	= electrical conductivity of glass at temperature $T_0$ (S/m)

## References

- <sup>1</sup>Kenneth R. Routt, **Modeling Principles Applied to the Simulation of a Joule-Heated Glass Melter**, U.S. Department of Energy Report DP-1540, E. I. du Pont de Nemours & Co., Savannah River Laboratory, Aiken, SC, (May 1980).
- <sup>2</sup>J. J. Noble, et al., "Mathematical and Experimental Modeling of the Circulation Patterns in Glass Melts," **Journal of Heat Transfer**, p 149 (May 1972).
- <sup>3</sup>N. W. E. Curlet, "Experimental and Numerical Modeling of Three-Dimensional Natural Convection in an Enclosure," **D. Sc. Thesis**, Massachusetts Institute of Technology (March 1976).
- <sup>4</sup>L. A. Clomburg, Jr., "Mathematical and Experimental Modeling of the Circulation Patterns in Glass Melts," **D. Sc. Thesis**, Massachusetts Institute of Technology (August 1971).
- <sup>5</sup>J. Stanek, **Electric Melting of Glass**, Elsevier Scientific Publishing Company, New York (1977).

TABLE I. Electrical Parameters Predicted by the Model

Parameter	Model*	Melter**
Electrode Power		
- AC electrodes (kW)	73	70
- BD electrodes (kW)	73	70
Electrode Potential		
- AC electrodes (volts)	39	48
- BD electrodes (volts)	39	48
Electrode Current		
- AC electrodes (A)	1864	1456
- BD electrodes (A)	1864	1456
Melt Pool Resistance		
- A to C electrode (ohms)	0.021	.033
- B to D electrode (ohms)	0.021	.033
Nominal Current Flux		
- AC electrodes (A/cm <sup>2</sup> )	0.68	0.53
- BD electrodes (A/cm <sup>2</sup> )	0.68	0.53

\* Melt rate of 40-51 kg/hr

\*\* Melt rate of 189 kg/hr

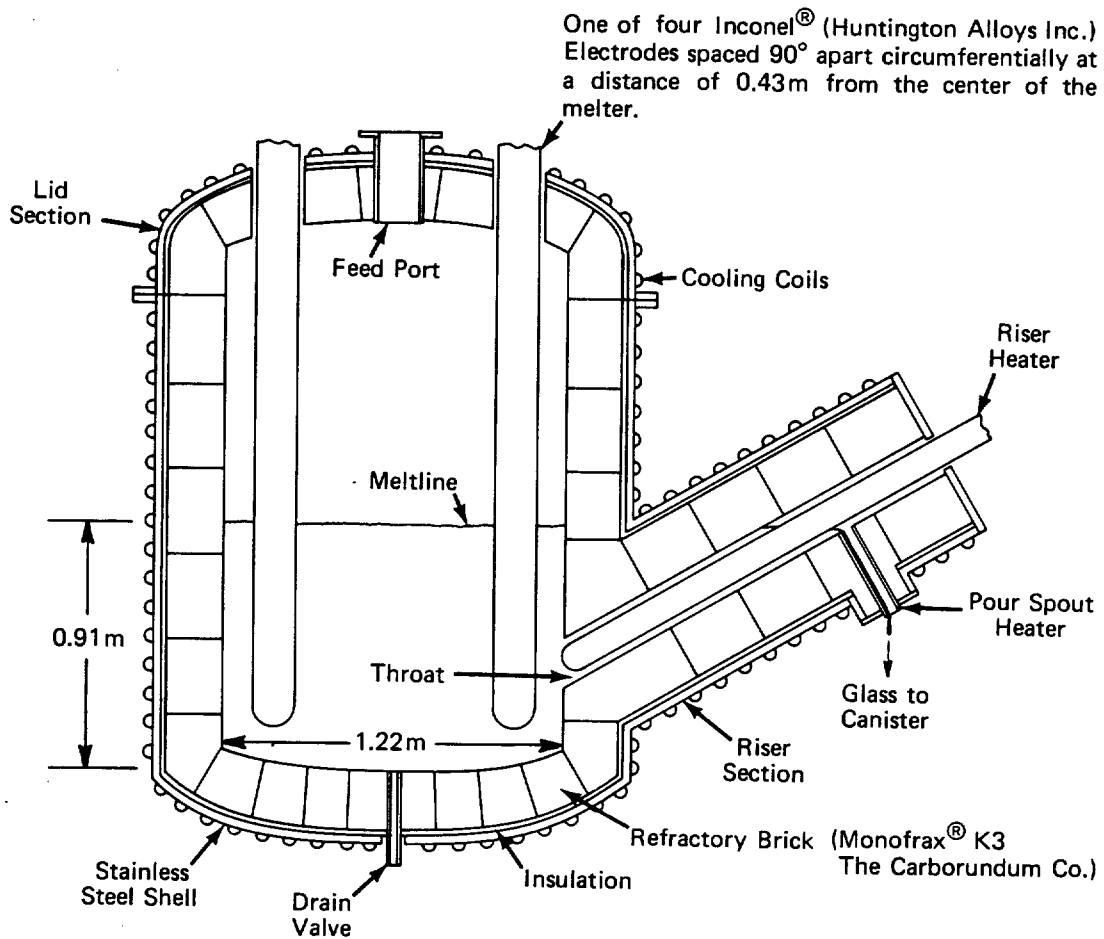


Fig. 1. Vertical section of glass melter. Power is supplied by a three-phase to two-phase Scott-Taylor transformer.

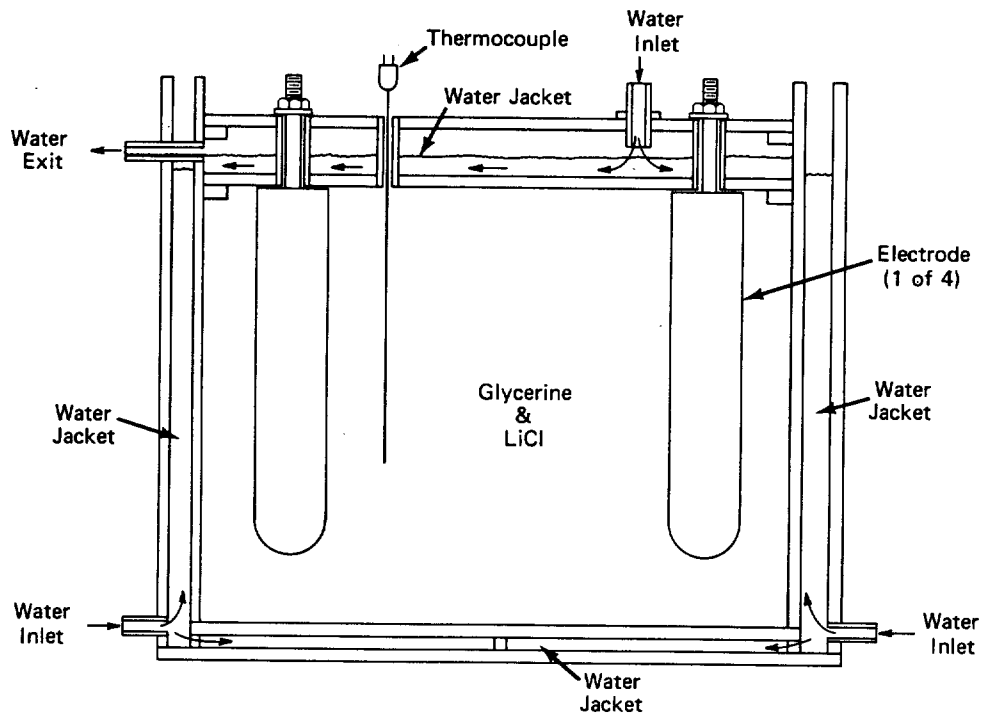


Fig. 2. Vertical section through model.

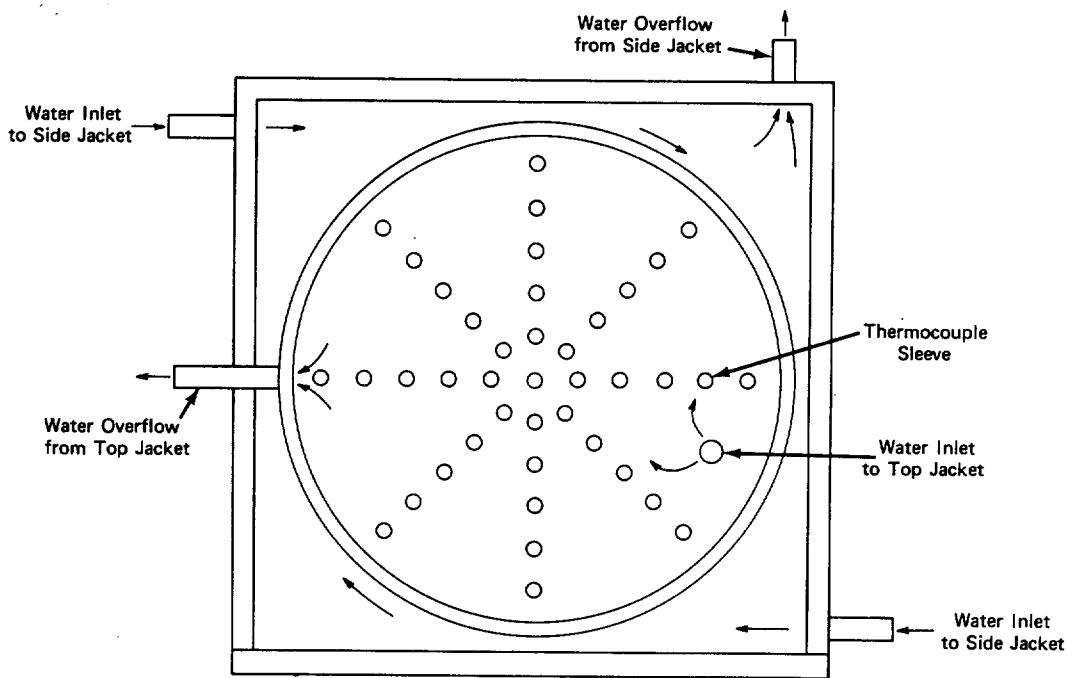


Fig. 3. Top view of model.

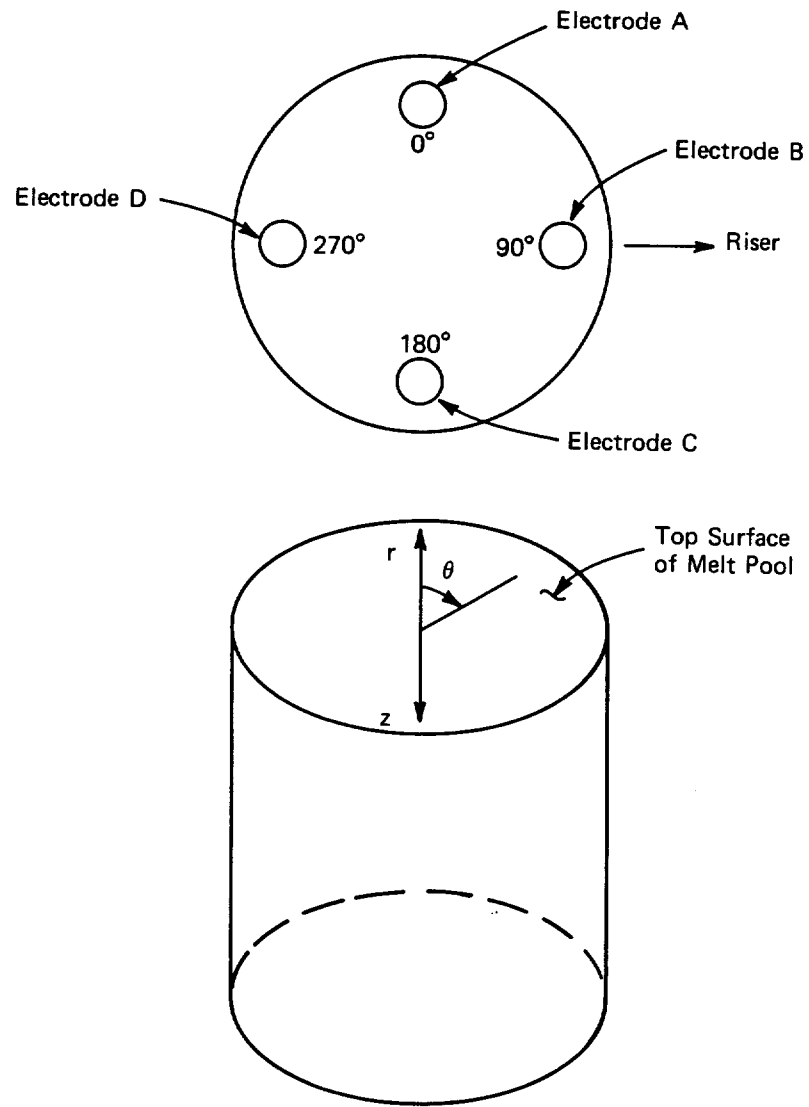


Fig. 4. Cylindrical coordinate system used for melter and model.

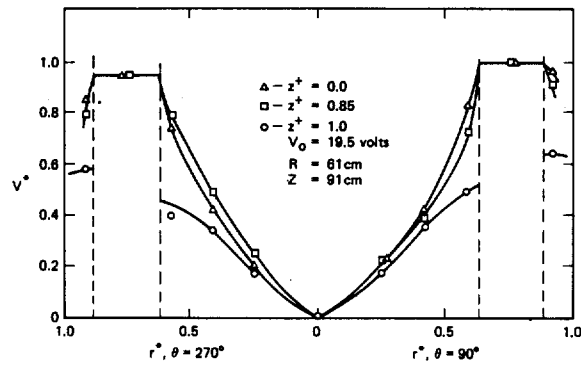


Fig. 5. Radial voltage profiles in the B-D electrode plane.

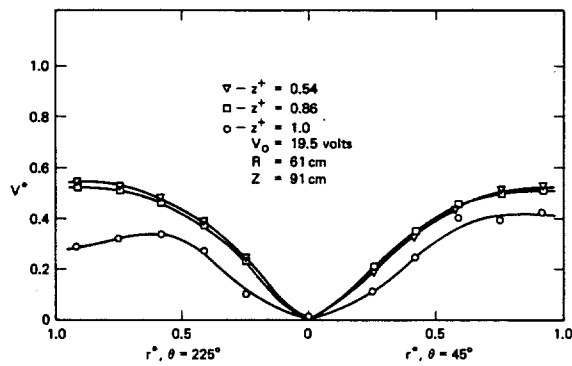


Fig. 6. Radial voltage profiles in a vertical plane between electrodes.

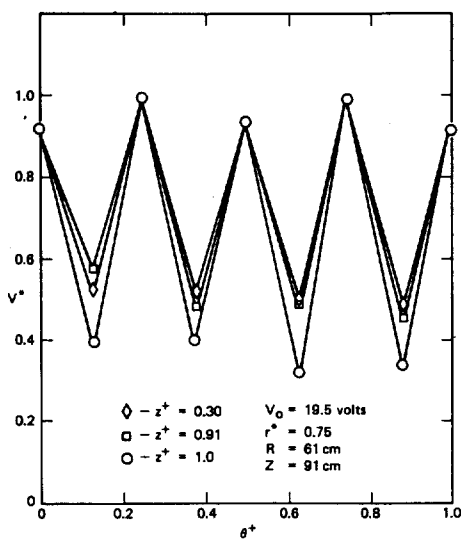


Fig. 7. Azimuthal voltage profiles.

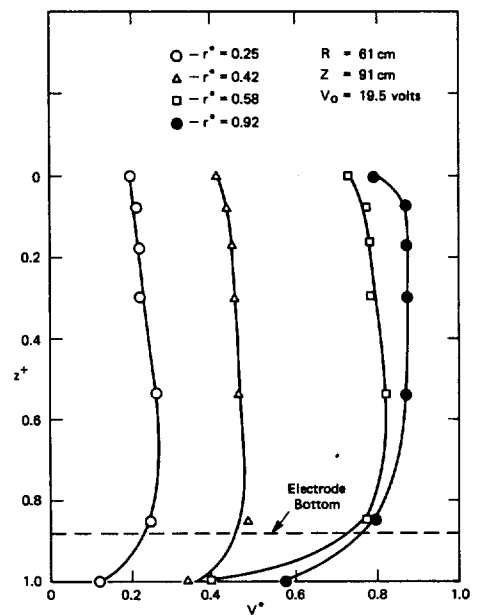


Fig. 8. Vertical voltage profiles.



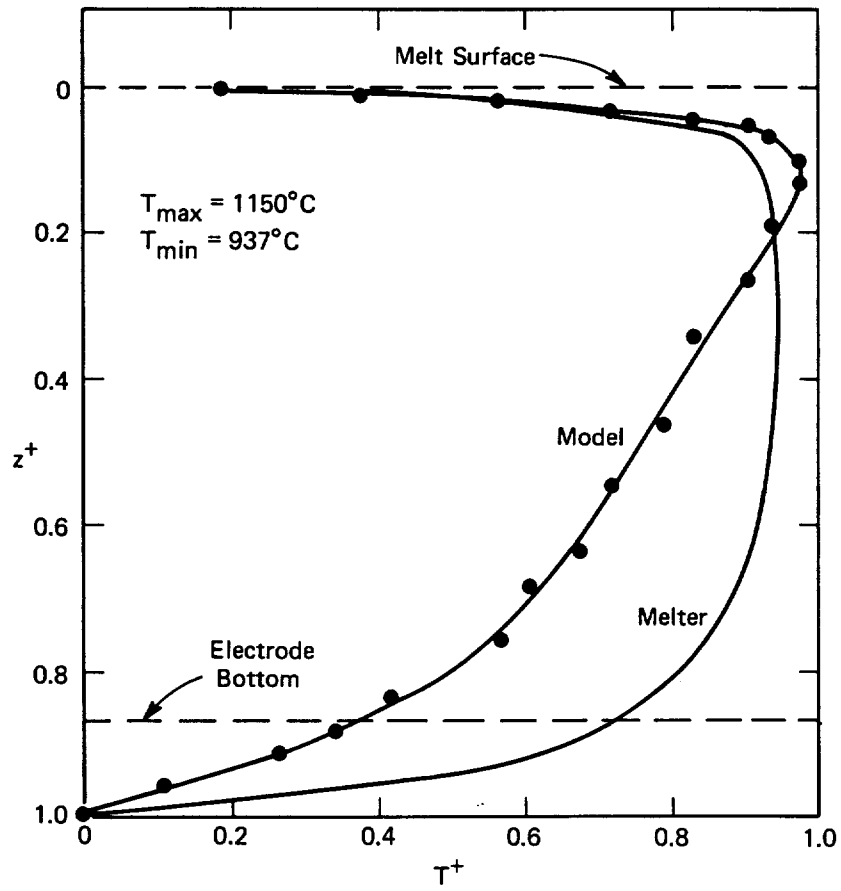


Fig. 11. Comparison of vertical temperature profiles in model and melter.

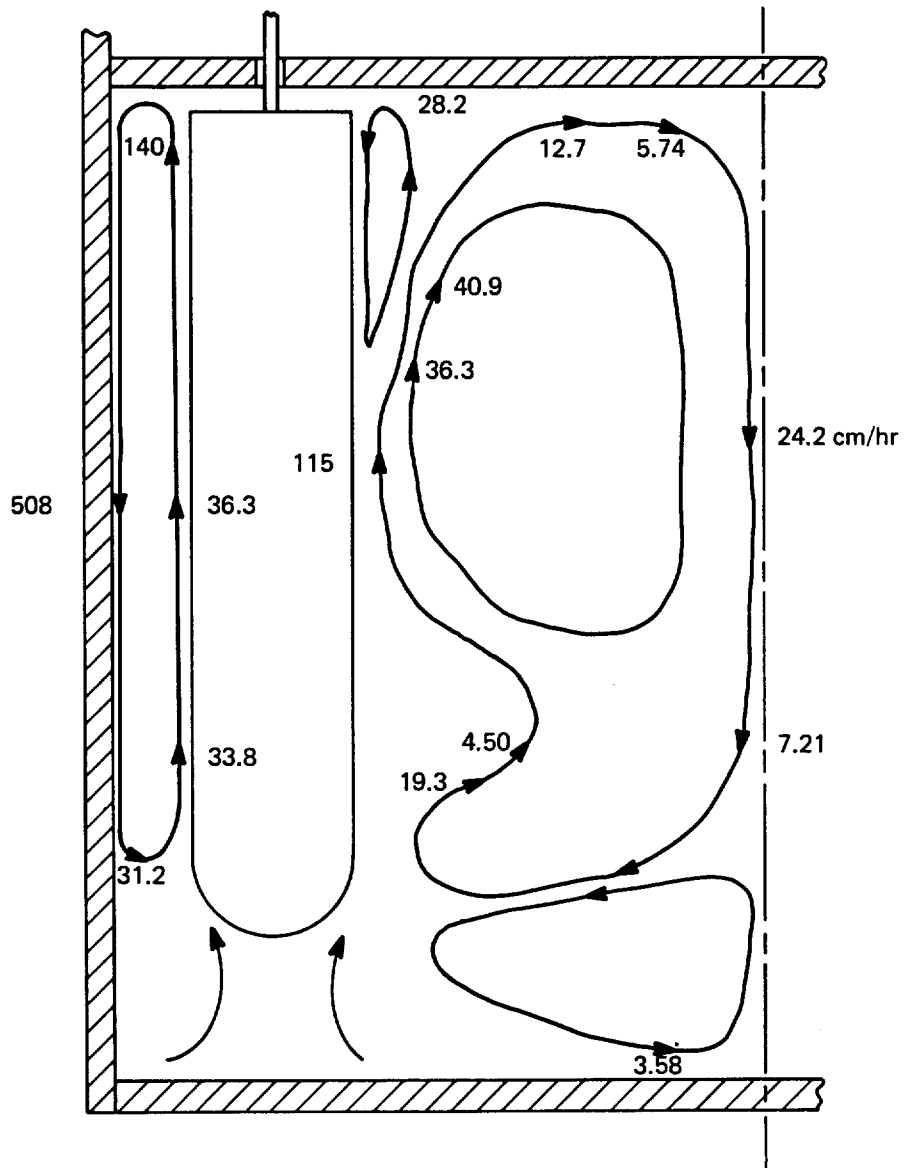


Fig. 12. Predicted velocities in the glass melter.